Associative ionization in collisions of $H^+ + H^-$ and $H(1s) + H(ns)$

Johan Hörnquist,[1,*] Patrik Hedvall,[1] Ann E. Orel,[2] and Åsa Larson[1]
[1]*Department of Physics, Stockholm University, AlbaNova University Center, SE-106 91 Stockholm, Sweden*
[2]*Department of Chemical Engineering, University of California, Davis, California 95616, USA*

(Received 8 September 2023; accepted 31 October 2023; published 13 November 2023)

Associative ionization in collisions of $H^+ + H^-$ as well as $H(1s) + H(ns)$ with $n = 2, 3, 4$ is studied theoretically. Relevant adiabatic potential curves and nonadiabatic couplings are calculated *ab initio* and the autoionization from the lowest electronic resonant states in the $^1\Sigma^+_{g/u}$ and $^3\Sigma^+_{g/u}$ symmetries are considered. The cross sections are obtained by solving the coupled Schrödinger equation, including a complex potential matrix, in a strict diabatic representation. The importance of using a nonlocal description of autoionization is investigated. Associative ionization is also studied for different isotopes of hydrogen. Calculated cross sections are compared with results from measurements.

DOI: 10.1103/PhysRevA.108.052811

I. INTRODUCTION

Associative ionization (AI) is a reactive scattering process where the translational energy of the colliding atoms is transferred into kinetic energy of a free electron, resulting in a molecular ion in its ground or excited rovibrational state. Here, we are interested in the following AI processes:

$$H(1s) + H(ns) \rightarrow H_2^+ + e^-, \tag{1}$$

where $n = 2$, 3, or 4, and

$$H^+ + H^- \rightarrow H_2^+ + e^-. \tag{2}$$

We also study the corresponding reactions where one or two of the hydrogen atoms or ions are replaced by deuterium. The main reaction mechanism by which these processes take place is through autoionization from doubly excited (resonant) states of the H_2 reaction complex. At low collision energies, the reaction predominantly proceeds via the lowest-lying resonant state of $^1\Sigma^+_g$ symmetry, which crosses the potential of H_2^+ close to its minimum. The situation is more complex at higher energies where there are several resonant states, of different electronic symmetries, that contribute. A theoretical treatment of these processes requires not only the potentials of these resonant states and their couplings to bound electronic states and the ionization continuum, but also the nonadiabatic couplings between the bound electronic states at various internuclear distances.

An understanding of the full dynamics of the AI process may offer valuable insight into the reverse processes dissociative recombination and ion-pair formation, and more specifically into the branching fractions of the former. Another interesting aspect is that AI between two metastable $\overline{H}(2s)$ atoms has been considered as a possible pathway of producing the antimatter counterpart of H_2^+ [1], which can be utilized to perform sensitive tests of the charge parity time (CPT) theorem [2]. There is also a possibility that process (1) with $n = 3$ and $n = 4$ could be used for this purpose, owing to the relatively large cross sections at small collision energies [3]. One advantage of using this alternative pathway to $\overline{H}_2^-$ would be that the competing process of collisional ionization is not energetically allowed at the small collision energies considered.

Associative ionization in collisions of hydrogen atoms is also important in astrophysics. Process (1) [with $H(ns)$ replaced by $H(n)$] has been found to be a major contributor to the formation of H_2^+ in astrophysical environments that depart from local thermodynamic equilibrium. For instance, it has been found to be an important intermediate step in the formation of H_2 in the outflow of young stellar objects [4] and for the formation of H_3^+ in the envelope of supernovae [5]. Together with collisional ionization, it is also of importance in the physics of stellar atmospheres [6–8].

The first and so far the only measurement on AI of two oppositely charged hydrogen ions [reaction (2)] was performed by Poulaert *et al.* [9] in 1978 using a merged beam apparatus. On the theoretical side, a calculation of the cross section of process (2) was performed by Urbain *et al.* [10], using multichannel quantum defect theory (MQDT), where they included the contributions from the molecular states of $^1\Sigma^+_g$ symmetry. Their calculation did not include the nonadiabatic couplings at large internuclear distances ($R > 8\,a_0$), but instead they selected the entrance channel in the autoionization region based on the most likely pathway according to the Landau-Zener probabilities at the curve crossings between the ion-pair state and the covalent $n = 3$ and $n = 2$ states. Despite this approximative treatment of the dynamics, they were able to capture the essential features as well as the magnitude of the measured cross section. Process (1) with $n = 2$ has been measured by Urbain *et al.* [11]. An interesting feature in the measured

*johan.hornquist@fysik.su.se

Published by the American Physical Society under the terms of the Creative Commons Attribution 4.0 International license. Further distribution of this work must maintain attribution to the author(s) and the published article's title, journal citation, and DOI. Funded by Bibsam.

cross section is a local minimum around 2 eV. This minimum was explained as arising from an interference between the two possible pathways along the diabatic $2s$ and $2p$ states, which are degenerate at large internuclear distances. They also provided an MQDT calculation of the cross section which supported this idea. Their calculated cross section is overall in good agreement with the measured one. In the high-energy range they underestimate the cross section which is due to their first-order treatment of loss due to the $H + H(n \geqslant 3)$ channels. The cross section of process (1) with $n = 3$ has been measured by Nehari *et al.* [12]. They also performed a semiclassical calculation of the cross section where they considered the contribution from the $^1\Sigma_g^+$ symmetry. This calculation was able to reproduce some of the main features of the cross section, but failed to reproduce the magnitude. This is in part due to the neglect of the other symmetries. Process (1) with $n = 4$ has been measured by Brouillard *et al.* [3], but no calculations of the cross section have been published as far as we know.

In this paper, we study processes (1) and (2) using a close-coupling approach in a strict diabatic representation. In our treatment we include the contributions from all the possible symmetries $^1\Sigma_{g/u}^+$ and $^3\Sigma_{g/u}^+$. Nonlocal effects, which may be important at low collision energies, are included using an iterative method. Whereas the autoionization occurs at small internuclear distances where the resonant states are embedded in the ionization continuum, transitions between bound electronic states of H_2 may occur at all ranges of internuclear distance where the nonadiabatic couplings are significant in size. In order to include the full long-range dynamics of the AI process it is thus important to include these couplings. We have previously performed *ab initio* calculations of the adiabatic potential curves and nonadiabatic couplings of states of $^1\Sigma_{g/u}^+$ symmetries, among others, correlating with the $n \leqslant 4$ asymptotic limits [13]. Here, we extend these calculations to also include the three lowest states of $^3\Sigma_u^+$ symmetry.

The outline of the paper is as follows. In Sec. II, the adiabatic potential curves and nonadiabatic couplings of the relevant states are discussed. Details of the nuclear dynamics calculations are also presented in this section. The results are presented and discussed in Sec. III. Throughout the paper atomic units are used, unless otherwise stated.

II. THEORY

A. Potential curves and couplings

The possible symmetries contributing to process (1) are $^1\Sigma_g^+$, $^3\Sigma_g^+$, $^1\Sigma_u^+$, and $^3\Sigma_g^+$, while only the singlet symmetries have an ion-pair state contributing to process (2). In order to calculate the cross sections of these processes, it is essential to include accurate data not only of the position and width of the relevant resonant states, but also the adiabatic potential curves and nonadiabatic couplings associated with these symmetries. We have previously computed accurate *ab initio* adiabatic potential curves and nonadiabatic couplings (including rotational couplings), diabatic quantum defects, as well as the potentials and autoionization widths of the lowest resonant states in the $^1\Sigma_{g/u}^+$ symmetries [13]. In the present work, we extend these calculations to also include triplet states. For the $^3\Sigma_u^+$ symmetry, we perform *ab initio* multireference configuration interaction (MRCI) calculations to obtain the adiabatic potential curves and nonadiabatic couplings of the three lowest states. We use the same basis set [13] as in our previous study. The molecular orbitals are obtained from state-averaged complete active space self-consistent field (CASSCF) calculations using an active space consisting of all molecular orbitals composed of the $n \leqslant 3$ atomic orbitals ($6\sigma_g$, $3\pi_g$, $1\delta_g$, $6\sigma_u$, $1\pi_u$, and $1\delta_u$ orbitals). The reference configurations of the MRCI calculation were generated using the same active space, and single and double external excitations out of the reference configurations were included. The lowest resonant state in this symmetry diabatically connects with the $n = 2$ asymptotic limit. The two states correlating with the $H(1s) + H(2s)$ and $H(1s) + H(2p)$ asymptotic limits are degenerate at large internuclear distances, and it is essential to include the nonadiabatic coupling between these two states for a good description of the $2s$ AI process. For the $^3\Sigma_g^+$ symmetry, on the other hand, the lowest resonant state diabatically connects with the $n = 3$ limit. We were not able to obtain the nonadiabatic couplings needed for all the states that correlate with this limit. Therefore, we use a quasidiabatic representation of the potentials in this symmetry. Since the lowest resonant state of the $^3\Sigma_g^+$ symmetry does not directly couple to the $n = 2$ states, we are therefore not able to obtain the cross section for the $2s$ process in this symmetry. Given that this resonant state does not directly couple to the $n = 2$ states and that the autoionization width is small, the contribution to the $2s$ AI cross section will likely be small.

In addition to the radial nonadiabatic couplings, there are also rotational couplings that couple electronic states that differ in the quantum number Λ (projection of the electronic orbital angular momentum onto the molecular axis) by one unit. These couplings were considered in our previous study of mutual neutralization [13]. We have included rotational couplings in preliminary calculations of the cross sections of processes (1) and (2) and it was found that their inclusion has a negligible influence on the cross sections (the relative difference was at most 3% at the energies considered). They are therefore neglected in the final calculations presented in this paper.

In our previous study [13], we have performed electron scattering calculations to include the lowest resonant states of $^1\Sigma_{g/u}^+$ symmetries. To determine the potentials of the lowest resonant states in the $^3\Sigma_{g/u}^+$ symmetries as well as total and partial autoionization widths, we have performed electron scattering calculations using the complex Kohn variational method [14] with a similar basis set as described in Ref. [13]. While the scattering calculations are performed for geometries where the potentials of the resonant states lie above the ion potential, we use the optimization procedure described in Ref. [13] for geometries where the resonant states have crossed the ion. Here we used the accurate adiabatic potential curves calculated by Kurokawa *et al.* [15] for excited states in $^3\Sigma_{g/u}^+$ symmetries.

While the adiabatic potential curves and nonadiabatic couplings can be used to describe the dynamics among the bound electronic states at both small and large internuclear distances, a quasidiabatic model is introduced in order to describe autoionization, which occurs at small internuclear distances. In this model we include the lowest resonant state and an

arbitrary number of Rydberg states in a given symmetry. We let the Rydberg states couple to the resonant state but assume there are no couplings among the Rydberg states. The potentials of the Rydberg states are given by the Rydberg formula

$$V_i(R) = V_{\rm ion}(R) - \frac{1}{2\left[n_i - \mu_l^d(R)\right]^2}, \tag{3}$$

where $\mu_l^d(R)$ is the diabatic quantum defect, n_i is the principal quantum number, and l is the orbital angular momentum quantum number of the outer electron. The couplings between the resonant state and the Rydberg states are given by the scaling relation [16]

$$V_{ri}(R) = \sqrt{\frac{\Gamma_l(R)}{2\pi}}\left[n_i - \mu_l^d(R)\right]^{-3/2}, \tag{4}$$

where $\Gamma_l(R)$ is the partial autoionization width. We consider the s and d partial autoionization widths in $^1\Sigma_g^+$ symmetry, p and f partial autoionization widths in $^1\Sigma_u^+$ and $^3\Sigma_u^+$ symmetries, and the s partial autoionization width in $^3\Sigma_g^+$ symmetry. The total autoionization width is given by the sum of the partial widths, $\Gamma(R) = \sum_l \Gamma_l(R)$. Using these definitions, a quasidiabatic potential matrix is set up and diagonalized. The adiabatic potentials, obtained via the transformation $\mathbf{V}^{ad} = \mathbf{S}^T\mathbf{V}^{qd}\mathbf{S}$, approximates the Born-Oppenheimer adiabatic potentials at small internuclear distances. From the transformation matrix $\mathbf{S}$, it is possible to obtain approximative nonadiabatic couplings for these potentials. In order to connect the short-range electronic interactions responsible for autoionization with the interactions arising from nonadiabatic couplings at various internuclear distances, the approximative adiabatic potentials and nonadiabatic couplings are combined with those calculated *ab initio*. The resulting adiabatic potentials are illustrated in Figs. 1 and 2.

The adiabatic potentials are then transformed to a strict diabatic representation by the transformation $\mathbf{V}^d = \mathbf{T}^T\mathbf{V}^{ad}\mathbf{T}$. The adiabatic to diabatic orthogonal transformation matrix $\mathbf{T}$ is a solution of the equation [17]

$$\left(\mathbf{I}\frac{d}{dR} + \boldsymbol{\tau}(R)\right)\mathbf{T}(R) = \mathbf{0}, \tag{5}$$

where $\mathbf{I}$ is the identity matrix and $\boldsymbol{\tau}$ is a matrix consisting of the first derivative nonadiabatic couplings. Within the Born-Oppenheimer approach, it is a well-known problem that some nonadiabatic couplings do not go to zero asymptotically [18]. This induces transitions between electronic states at arbitrarily large internuclear distances. The effect can be significant if the asymptotic values of the couplings are large, but can readily be dealt with using the reprojection method [18–21]. Applying this method in the present case, it was found that the asymptotic values of the nonadiabatic couplings are too small to significantly influence the cross sections (the relative difference was found to be at most 5% and on average 0.7%). In the asymptotic region, we therefore assume that all the first derivative nonadiabatic couplings go to zero and that $\mathbf{T}$ is equal to the identity matrix.

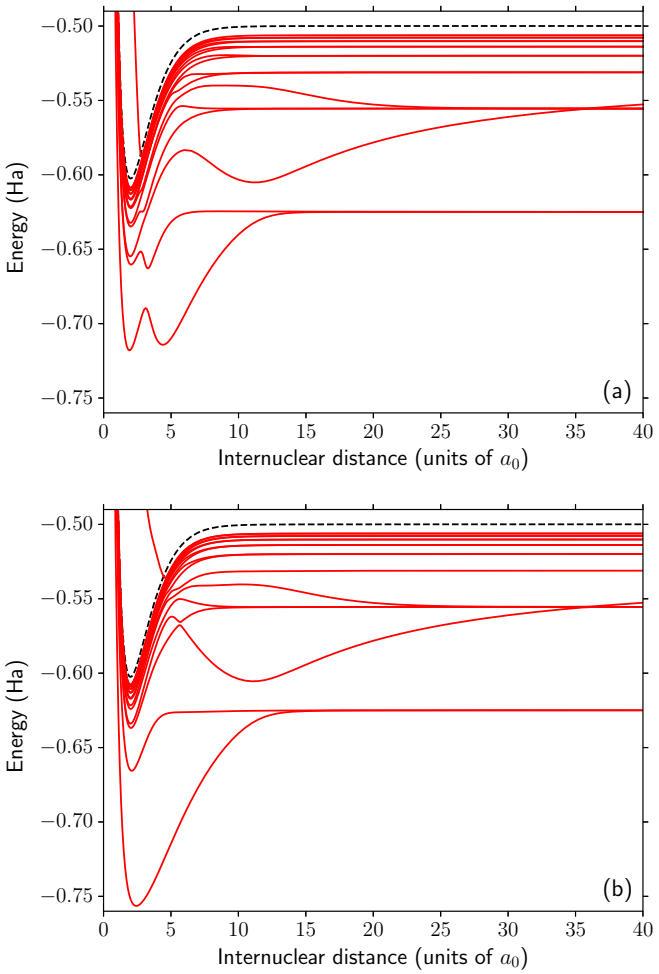

FIG. 1. Adiabatic potential energy curves of (a) $^1\Sigma_g^+$ and (b) $^1\Sigma_u^+$ symmetries. The ground state potential is not shown in (a).

B. Nuclear dynamics

To study the AI process, we use a close-coupling approach. In order to allow for loss due to autoionization we use a complex Schrödinger equation which is derived using the P and Q projection operator formalism [22,23]. We let $|\phi_i\rangle$ represent the bound electronic states and $|\phi_{\bar{\epsilon}}\rangle$ represent the electronic continuum. A division of the electronic Hamiltonian is obtained by introducing the two projection operators Q and P,

$$Q = \sum_i |\phi_i\rangle\langle\phi_i|, \quad P = \int d\bar{\epsilon}|\phi_{\bar{\epsilon}}\rangle\langle\phi_{\bar{\epsilon}}|. \tag{6}$$

Writing the total wave function as $|\Psi\rangle = Q|\Psi\rangle + P|\Psi\rangle$, we find

$$\begin{aligned} P(E-H)P|\Psi\rangle &= PHQ|\Psi\rangle, \\ Q(E-H)Q|\Psi\rangle &= QHP|\Psi\rangle. \end{aligned} \tag{7}$$

By considering only outgoing waves in the P space, these two equations lead to a coupled Schrödinger equation for the nuclear states of the Q space. This equation contains a nonlocal operator which is given by

$$F_{ij}^+(\vec{R},\vec{R}') = \langle\phi_i|HPG_P^+(\vec{R},\vec{R}')PH|\phi_j\rangle, \tag{8}$$

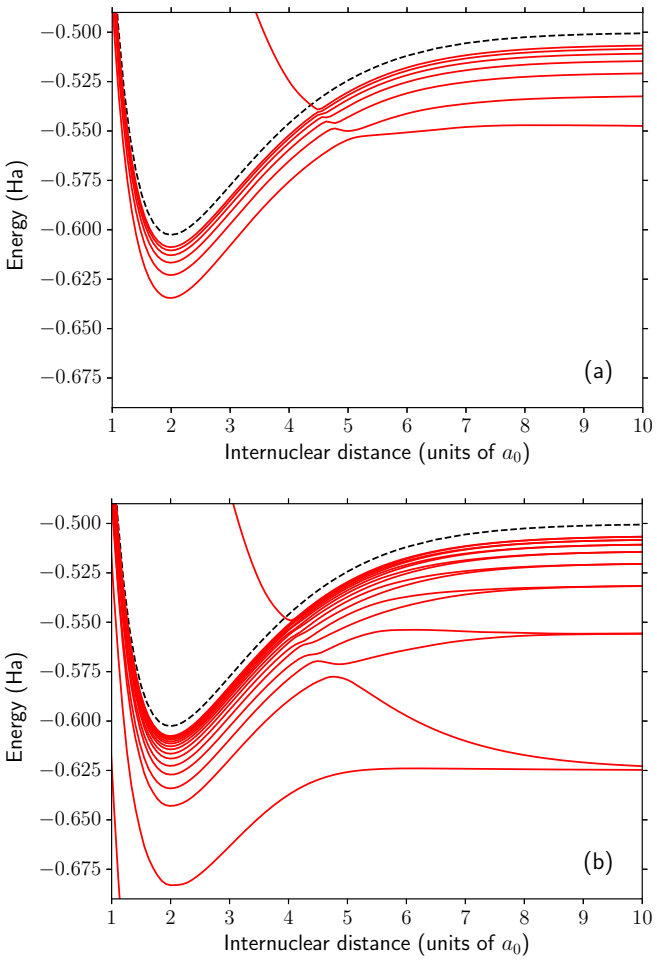

FIG. 2. Adiabatic potential energy curves of (a) $^3\Sigma_g^+$ and (b) $^3\Sigma_u^+$ symmetries. In (b), the potential of the lowest state is not shown.

where G_P^+ is the Green's operator corresponding the the homogeneous P-space equation. The nuclear kinetic energy operator, which is contained in H, will introduce first and second derivative couplings between the Q and P spaces. These sorts of couplings describe the indirect mechanism and are usually neglected in the close-coupling equations. This is also done in the present case.

By extending the work of Bieniek [24] to the multichannel case, using a strict diabatic representation, we can derive the coupled Schrödinger equation, which takes the form

$$\frac{d^2}{dR^2}\mathbf{\Psi}^J(R) + \mathbf{f}^J(R)\mathbf{\Psi}^J(R) = \int dR' \mathbf{g}(R,R')\mathbf{\Psi}^J(R'), \quad (9)$$

where J is the angular momentum quantum number of the formed molecular complex, $\mathbf{\Psi}$ is the wave function matrix, and $\mathbf{f}^J$ is given by

$$f_{ij}^J(R) = 2\mu\left[E\delta_{ij} - \frac{J(J+1)}{2\mu R^2}\delta_{ij} - V_{ij}^d(R)\right]. \quad (10)$$

Since we are studying processes (1) and (2) for different isotopes of the hydrogen atoms and ions, different values are used for the reduced mass μ. The diabatic potential matrix is given as a transformation, $\mathbf{V}^d = \mathbf{T}^T\mathbf{V}^{ad}\mathbf{T}$, of the adiabatic potential matrix. Equation (9) contains a nonlocal potential on the right-hand side which is imaginary and is responsible for loss due to autoionization. Explicitly, we have [16,25]

$$g_{ij}(R,R') = -i\mu \sum_{mn\nu J'l} (2J'+1)\begin{pmatrix} J & J' & l \\ 0 & 0 & 0 \end{pmatrix}^2 \times T_{im}^T(R)S_{mr}^T(R)\sqrt{\Gamma_l(R)}\chi_\nu^{J'}(R) \times \chi_\nu^{J'}(R')\sqrt{\Gamma_l(R')}S_{rn}(R')T_{nj}(R'). \quad (11)$$

The sum over m and n runs over the diabatic states, ν over the vibrational channels of H_2^+ that are open at a given collision energy, l over the angular momentum quantum number of the ejected electron, and J' over the angular momentum of the ion. The subscript r refers to the resonant state. In the present case, the resonant state potential in a given symmetry crosses the ion potential at an internuclear distance R_c. This means that there is some portion of the vibrational channels that are closed at low collision energies. An approximation commonly applied is the assumption that the open vibrational channels form a complete set at any energy, i.e., that $\sum_\nu \chi_\nu^{J'}(R)\chi_\nu^{J'}(R') = \delta(R-R')$, which leads to the so-called local approximation [26–29]. Carrying out the integral on the right-hand side of Eq. (9) under this assumption, one finds that

$$\frac{d^2}{dR^2}\mathbf{\Psi}^J(R) + \mathbf{f}^J(R)\mathbf{\Psi}^J(R) = \mathbf{W}(R)\mathbf{\Psi}^J(R). \quad (12)$$

The matrix $\mathbf{W}(R)$ is now a local complex potential given by

$$W_{ij}(R) = -i\mu \sum_{mn} T_{im}^T(R)S_{mr}^T(R)\Gamma(R)S_{rn}(R)T_{nj}(R), \quad (13)$$

where $\Gamma(R)$ is the total autoionization width. The local approximation is expected to be less valid for low collision energies where a large portion of the vibrational channels are closed. By having these two sets of equations, we can test the validity of this approximation.

Once Eq. (9) has been solved for the nuclear wave functions, $\mathbf{\Psi}^J(R)$, the partial cross section going from an initial state of J to a final state of J' and ν can be calculated from the expression [24]

$$\sigma\left(E, E_\nu^{J'}\right) = g\frac{4\pi^3}{k_i^2}(2J'+1)\sum_{Jl}(2J+1)\begin{pmatrix} J & J' & l \\ 0 & 0 & 0 \end{pmatrix}^2 \times \left|\sum_{mn}\left\langle\chi_\nu^{J'}\middle|T_{mn}(R)S_{rm}(R)\sqrt{\frac{\Gamma_l(R)}{2\pi}}\middle|\psi_{ni}^J\right\rangle\right|^2, \quad (14)$$

where i is the initial state. To obtain the total AI cross section, the partial cross sections $\sigma(E, E_\nu^{J'})$ are summed over all quantum numbers J' and ν of all final rovibrational states that are energetically open.

Equation (9) is an integro-differential equation. Here we apply an iterative procedure to solve this equation, i.e., we solve the equation

$$\frac{d^2}{dR^2}\mathbf{\Psi}_i^J(R) + \mathbf{f}^J(R)\mathbf{\Psi}_i^J(R) = \int dR' \mathbf{g}(R,R')\mathbf{\Psi}_{i-1}^J(R'). \quad (15)$$

As a first guess of the wave function matrix to start the iteration, we use the local wave function $\mathbf{\Psi}_0^J(R)$ found by

solving Eq. (12) using the renormalized Numerov method [30]. Since the wave function from the previous step is known, the right-hand side of Eq. (15) becomes a known function of R. The resulting inhomogeneous equation can be solved for the wave function matrix, $\mathbf{\Psi}_i^J(R)$, using an extension of the renormalized Numerov method [31]. Once $\mathbf{\Psi}^J(R)$ is known, the cross section is calculated from Eq. (14) by extracting the column of the wave function matrix that corresponds to the correct boundary conditions. When the relative difference of two successive partial cross sections is less than 10^{-5}, we consider the iteration to be converged. Applying the iterative method in test calculations, it was found that the partial cross sections calculated from the wave functions of (15) did not converge. In order to obtain convergence, the alternative equation

$$\frac{d^2}{dR^2}\mathbf{\Psi}_i^J(R) + \mathbf{f}^J(R)\mathbf{\Psi}_i^J(R) - \mathbf{W}(R)\mathbf{\Psi}_i^J(R) = \int dR'\mathbf{g}(R,R')\mathbf{\Psi}_{i-1}^J(R') - \mathbf{W}(R)\mathbf{\Psi}_{i-1}^J(R) \tag{16}$$

was used instead. Once a convergence is reached, the two terms containing the local complex potential cancel and a solution of Eq. (16) is therefore identical to a solution of Eq. (15). In all calculations, the average number of iterations needed to reach convergence was of the order of ten iterations.

C. Asymptotically degenerate states

In the asymptotic region, the excited states correlating with $n \geqslant 2$ are degenerate. This implies that the molecular states will be linear combinations of atomic states in this region. In order to select a specific initial state corresponding to some value of the quantum numbers (n, l, λ), one therefore has to determine this linear combination. Following the work of Ref. [32], we write the molecular electronic wave function as a linear combination of the degenerate atomic states

$$\mathbf{\Phi}_{\text{mol}} = \mathbf{B}\mathbf{\Phi}_{\text{at}}, \tag{17}$$

where the matrix $\mathbf{B}$ is orthogonal.

Equations that determine the $\mathbf{B}$ matrix can be set up by writing the *ab initio* calculated first derivative nonadiabatic couplings as linear combinations of the couplings calculated using an atomic basis. In an atomic basis, one has [18,19]

$$\langle\phi_i^{\text{at}}|\frac{\partial}{\partial R}|\phi_j^{\text{at}}\rangle_\infty = \gamma[V_i(\infty) - V_j(\infty)]\langle\phi_i^{\text{at}}|z|\phi_j^{\text{at}}\rangle, \tag{18}$$

where $\langle\phi_i^{\text{at}}|z|\phi_j^{\text{at}}\rangle$ are atomic transition dipole moment that can be calculated analytically using the eigenstates of atomic hydrogen. The factor γ is given by $1/2$ in the present case. Since the molecular states are written as linear combinations of atomic states with the same n, we can parametrize the $\mathbf{B}$ matrix by blocks of $n \times n$ orthogonal matrices. We neglect any mixing between the $n = 4$ states because not all of them are calculated *ab initio*. Therefore, we parametrize the $\mathbf{B}$ matrix using block matrices composed of 2×2 and 3×3 rotation matrices while the rest of the $\mathbf{B}$ matrix contains ones along the diagonal and zeros otherwise.

By using the notation $\overline{\tau}_{ij}^{\text{mol}}$ for the asymptotic values of the nonadiabatic couplings in a molecular basis and $\overline{\tau}_{ij}^{\text{at}}$ for those in an atomic basis, we have the relation

$$\overline{\tau}_{ij}^{\text{mol}} = \sum_{kl} B_{ik}\overline{\tau}_{kl}^{\text{at}}B_{jl}. \tag{19}$$

By using the selection rules for the hydrogen transition dipole moments, this set of equations was reduced further and was then minimized using least squares to obtain the relevant elements of the $\mathbf{B}$ matrix. The optimization was done separately for the symmetries $^1\Sigma_g^+$ and $^1\Sigma_u^+$. A comparison of the *ab initio* calculated nonadiabatic couplings of $^3\Sigma_u^+$ symmetry with the couplings calculated using Eq. (18) shows that there is no mixing among the $n = 2$ states in that symmetry, and the corresponding $\mathbf{B}$ matrix will therefore be equal to the identity matrix. Performing the optimization for the symmetries $^1\Sigma_g^+$ and $^1\Sigma_u^+$, we obtain the values of the elements of the $\mathbf{B}$ matrix as given in Tables I and II, respectively.

To include the $\mathbf{B}$ matrix in the nuclear dynamics calculations, one must modify the boundary conditions slightly. The new scattering matrix, which we denote by $\overline{\mathbf{S}}$, is written in terms of the old scattering matrix as $\overline{\mathbf{S}} = \mathbf{B}^T\mathbf{S}\mathbf{B}$. The corresponding boundary conditions are written as

$$\mathbf{\Psi}^J(R_N) \sim \hat{\mathbf{h}}_{J,N}^-\mathbf{B} - \hat{\mathbf{h}}_{J,N}^+\mathbf{B}\overline{\mathbf{S}}, \tag{20}$$

where $[\hat{h}_{J,N}^\pm]_{ij} = \frac{1}{\sqrt{k_j}}\hat{h}_J^\pm(k_jR_N)\delta_{ij}$ and where $\hat{h}_J^\pm$ are Riccati-Hankel functions (or the corresponding functions for Coulomb or closed channels).

TABLE I. The relevant elements B_{ij} of the $\mathbf{B}$ matrix for $^1\Sigma_g^+$ symmetry.

i \ j	2	3	4	5	6
2	0.9992	−0.0410	0	0	0
3	0.0410	0.9992	0	0	0
4	0	0	−0.0187	−0.0317	0.9993
5	0	0	−0.0934	−0.9951	−0.0333
6	0	0	0.9955	−0.0939	0.0157

III. RESULTS AND DISCUSSION

A. $H^+ + H^-$

Using the model described in Sec. II, we are able to add an arbitrary number of Rydberg states to our calculations. These additional states are expected to reduce the cross section because some flux is lost from the electronic autoionizing state

TABLE II. The relevant elements B_{ij} of the $\mathbf{B}$ matrix for $^1\Sigma_u^+$ symmetry.

i \ j	1	2	3	4	5
1	−0.1122	0.9937	0	0	0
2	−0.9937	−0.1122	0	0	0
3	0	0	0.0292	0.0184	−0.9994
4	0	0	0.0014	−0.9998	−0.0184
5	0	0	−0.9996	−0.0009	−0.0292

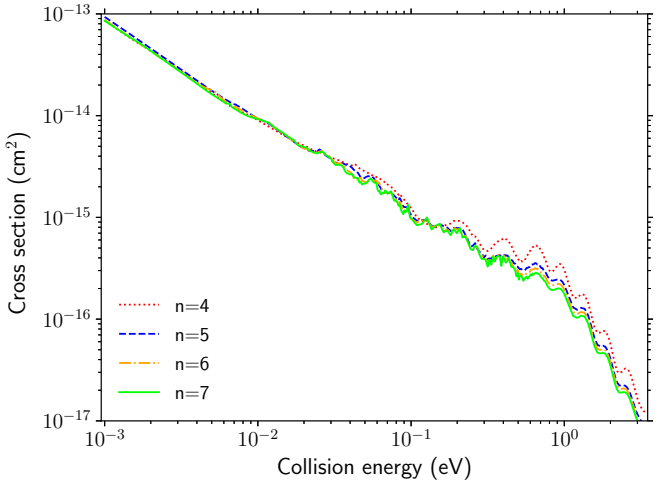

FIG. 3. Calculated $H^+ + H^-$ AI cross section obtained by including higher excited Rydberg states going to the asymptotic limits $n = 4, 5, 6, 7$.

to the bound Rydberg states. In Fig. 3, we show the total $H^+ + H^-$ AI cross section, obtained by a summation of the cross sections calculated in the $^1\Sigma_g^+$ and $^1\Sigma_u^+$ symmetries using a statistical weight of 1/2, including covalent states associated with the $n \leqslant 4, 5, 6, 7$ limits. The cross section is reduced whenever new states are added to the calculations. The reduction is largest when states correlating with the $n = 5$ limit are added and gradually becomes smaller for each new n. For $n = 7$, the cross section is converged with respect to the number of states that are included, and we see similar results in our calculations of the cross sections of process (1). The remaining results therefore include states up to the $n = 7$ limit, a total of 15 states of $^1\Sigma_g^+$ symmetry, 13 states of $^1\Sigma_u^+$ and $^3\Sigma_u^+$ symmetries, and five states of $^3\Sigma_g^+$ symmetry.

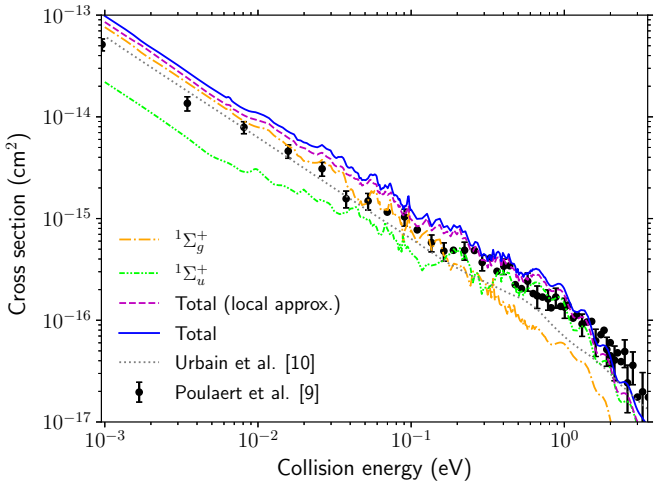

FIG. 4. Calculated $H^+ + H^-$ AI cross section: $^1\Sigma_g^+$ (dashed dotted orange), $^1\Sigma_u^+$ (densely dash-dot dotted green) and total (solid blue). The total cross section calculated with the local approximation is shown in dashed magenta. Also shown are the experimental result of Ref. [9] and calculated cross section of Ref. [10].

In Fig. 4, we show the $H^+ + H^-$ AI cross section calculated including states of $^1\Sigma_g^+$ and $^1\Sigma_u^+$ symmetries together with the total cross section. Also shown in the figure are the measured cross section by Poulaert *et al.* [9] and the calculated one by Urbain *et al.* [10]. The present result is in reasonably good agreement with the measured cross section, although it slightly overestimates it at low collision energies (about a factor of 2 below 0.2 eV). At low collision energies, the cross section goes as $1/E$, which is expected from Wigner's threshold law [33]. The $^1\Sigma_g^+$ symmetry is most important at low collision energies due to the favorable location of the resonant state potential. At higher energies, the $^1\Sigma_u^+$ symmetry becomes increasingly important. The rapid decrease of the cross section above 0.75 eV is due to competition with the collisional ionization process

$$H^+ + H^- \rightarrow H^+ + H + e^-, \tag{21}$$

which is not considered in the present study.

There are two different kinds of structures that appear in the cross section. First, we have sharp resonances that appear due to the inclusion of asymptotically closed states, which allows the system to become temporarily trapped in bound rovibrational states of the collision complex. The addition of angular momentum causes these resonances to be washed out. As is seen in Fig. 3, these resonances are not present in the $n = 4$ cross section since the $n \leqslant 4$ channels are open at the energies considered. Second, we have oscillations in the cross section which are due to interference between different pathways along the potential landscape. As shown in Fig. 4, these oscillations are largest in the $^1\Sigma_u^+$ symmetry. Using a set of quasidiabatic potentials, excluding the nonadiabatic couplings around 36 a_0 among the $n = 3$ states and the ion-pair state, no such oscillations are present in the cross section. Furthermore, a calculation including only the states $(3-6)^1\Sigma_u^+$ is able to reproduce the oscillations in the cross section. This suggests that the oscillations are due to accumulated phase differences along the possible paths among the $(3-6)^1\Sigma_u^+$ states.

We have investigated how important a nonlocal description of autoionization is by also performing a calculation using the local approximation [Eq. (12)], which is also shown in Fig. 4. Including a nonlocal potential slightly increases the cross section, which is due to less loss of flux into the ionization continuum. We see that in the case of $H^+ + H^-$ AI, the local approximation reproduces the experimental result well, especially for higher energies.

To investigate the isotope effect, we have also calculated the AI cross section in collisions of $H^+ + D^-$ and $D^+ + D^-$. The result is shown in Fig. 5. At low collision energies, the cross section increases as the reduced mass of the nuclei is increased, while the reverse is true at high collision energies.

B. H(1*s*) + H(4*s*)

The total $H(1s) + H(4s)$ AI cross section is shown in Fig. 6 together with the contribution from the different possible symmetries in comparison with the measured cross section of Ref. [3]. For this process, the $^1\Sigma_u^+$ and $^3\Sigma_u^+$ symmetries are the most important ones for the energy range considered here. The measured cross section displays a $1/E$ dependence at low collision energies, which is not reproduced in the calculated

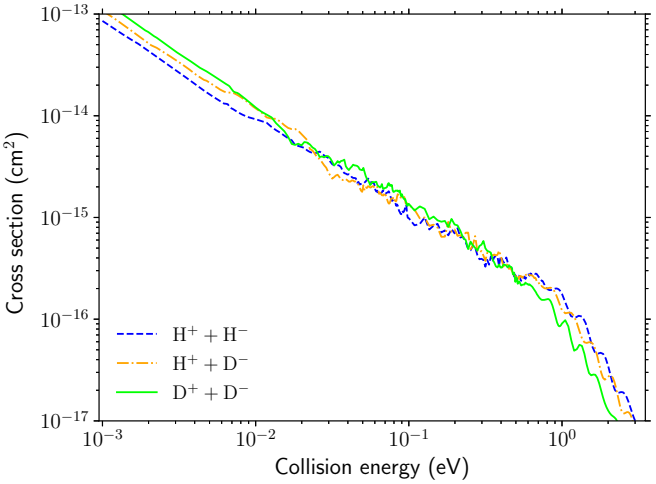

FIG. 5. Calculated AI cross sections for different isotopes of ionic hydrogen.

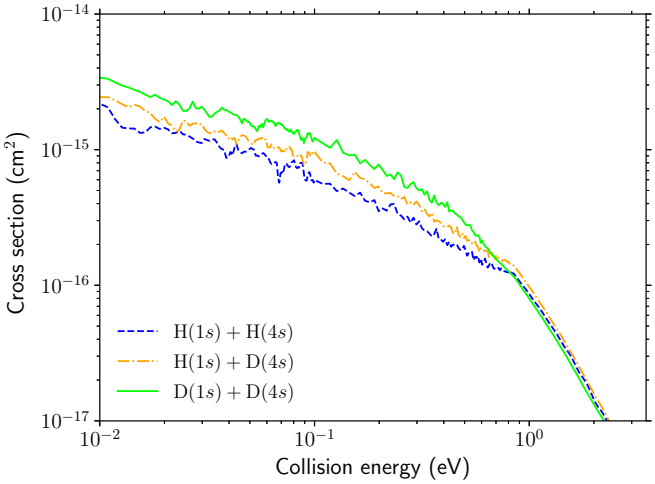

FIG. 7. Calculated 4s AI cross sections for different isotopes of atomic hydrogen.

cross section. At high energies, the present result is smaller than the measured cross section (about a factor of 6 at 1 eV and more at higher energies). This may be due to higher-lying resonant states that were not included in the calculation.

The present calculation of the total cross section does not reproduce the oscillations that are seen in the experimental cross section. These oscillations probably have an origin in terms of interference between different reaction pathways [3]. Such oscillations can be seen to some extent in the calculated $^1\Sigma^+_{g/u}$ cross sections, which are the only symmetries in which states correlating with the $n = 4$ limit are included in a strict diabatic representation. However, there are four states correlating with the $n = 4$ limit in each symmetry, out of which only two in the $^1\Sigma^+_g$ symmetry and one in the $^1\Sigma^+_u$ symmetry are included in the present calculation. In the triplet symmetries, the $n = 4$ states are included using a quasidiabatic representation. A better description of these states, including the relevant first derivative nonadiabatic couplings, would likely improve the present result.

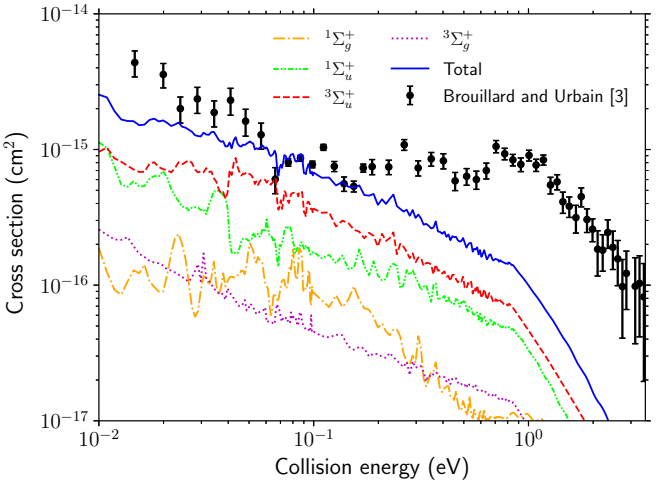

FIG. 6. Calculated H(1s) + H(4s) AI cross section in comparison with the experimental result of Ref. [3].

When one or both hydrogen atoms are replaced with deuterium, as seen in Fig. 7, we see a similar result in terms of the ordering of the cross sections as was seen in the case of ionic collision partners.

C. H(1s) + H(3s)

The H(1s) + H(3s) total AI cross section has been calculated for energies between 0.01 and 3.5 eV and the result is displayed in Fig. 8. For a better comparison with the experiment, the calculated total cross section is averaged with a Gaussian distribution over the experimental energy resolution [34]. At low collision energies, only the $^1\Sigma^+_g$ symmetry contributes. The $^3\Sigma^+_u$ and $^3\Sigma^+_g$ symmetries become important around 0.3 eV and 0.7 eV, respectively, while the $^1\Sigma^+_u$ cross section contributes mainly at higher energies. These

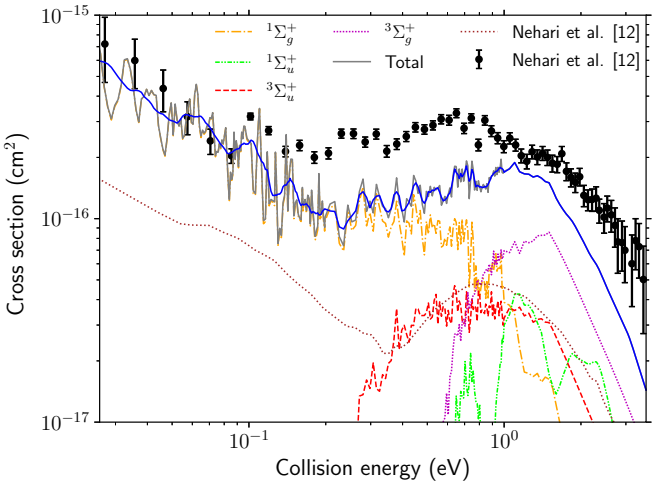

FIG. 8. Calculated H(1s) + H(3s) AI cross section. Also shown in the figure are the measured and calculated cross sections of Ref. [12]. The solid gray curve is the total cross section and the smoothed solid blue curve is the same data averaged over the experimental energy resolution.

symmetries are responsible for the increase in the total cross section, starting at a collision energy of about 0.2 eV. The rapid decrease of the cross section above 1.5 eV is due to competition with the collisional ionization process.

At intermediate energies, the total cross section displays a rich pattern of sharp resonances superimposed by oscillations which likely are due to competition between different pathways in the potential landscape. We are not able to reproduce the magnitude of the measured cross section in the region of energies between 0.2 and 0.8 eV, but the shape of the calculated cross section agrees well with the measured cross section. For the $^3\Sigma_u^+$ symmetry, our model is limited since we use a quasidiabatic description of the states correlating with the $n = 3$ asymptotic limit. Including the nonadiabatic couplings associated with these states would likely improve the present result. At higher energies, the disagreement between theory and experiment could be due to higher-lying resonant states not considered in the calculation. The present result is an improvement compared with the calculation by Nehari *et al.* [12], which is not surprising given the semiclassical nature of their calculation and the fact that they only included electronic states of $^1\Sigma_g^+$ symmetry.

We have also calculated the AI cross section in collisions of $H(1s) + D(3s)$ and $D(1s) + D(3s)$. The results of these calculations are shown in Fig. 9. The $H(1s) + H(3s)$ and $D(1s) + D(3s)$ experimental cross sections go as $1/E$ for low collision energies. This low-energy behavior, which is not typical for neutral reactants, has been proposed to arise from the requirement that the rotational energy of H_2^+ (or D_2^+) does not exceed its binding energy [3,12]. The calculated cross sections have the same behavior between 0.1 and 0.02 eV, but deviate from it for lower collision energies.

In Fig. 9(b), we compare the calculated $D(1s) + D(3s)$ AI cross section with the experimental result of Ref. [12]. There is a reasonable agreement with the experiment in terms of the magnitude and shape of the cross section, especially in the region 0.02–0.3 eV. At collision energies of about 0.7 eV and 1.6 eV, there are two distinct peaks in the experimental cross section which are not reproduced in the calculated cross section. It is possible that these peaks are due to higher-lying resonant states which have not been included in the present calculation.

D. H(1*s*) + H(2*s*)

In Fig. 10, the calculated $H(1s) + H(2s)$ AI cross section including contributions from the symmetries $^1\Sigma_g^+$ and $^3\Sigma_u^+$ is shown in comparison with previous theoretical [11] and experimental [11] results. The $^1\Sigma_u^+$ cross section is at most of the order of 10^{-21} cm^2 and is therefore neglected. At around 0.7 eV, the process has a threshold where the lowest rovibrational state of the ion becomes energetically open. The local minimum of the cross section around 2 eV results from an interference between the two pathways along the two potentials of $^1\Sigma_g^+$ symmetry that correlate with the $n = 2$ limit. In addition to the results shown in Fig. 10, we have performed a calculation of the cross section with the $2p$ state as the initial state. The result (not shown in the figure), do indeed oscillate 180 degrees out of phase with the $2s$ cross section, which demonstrates that this interpretation is correct. This

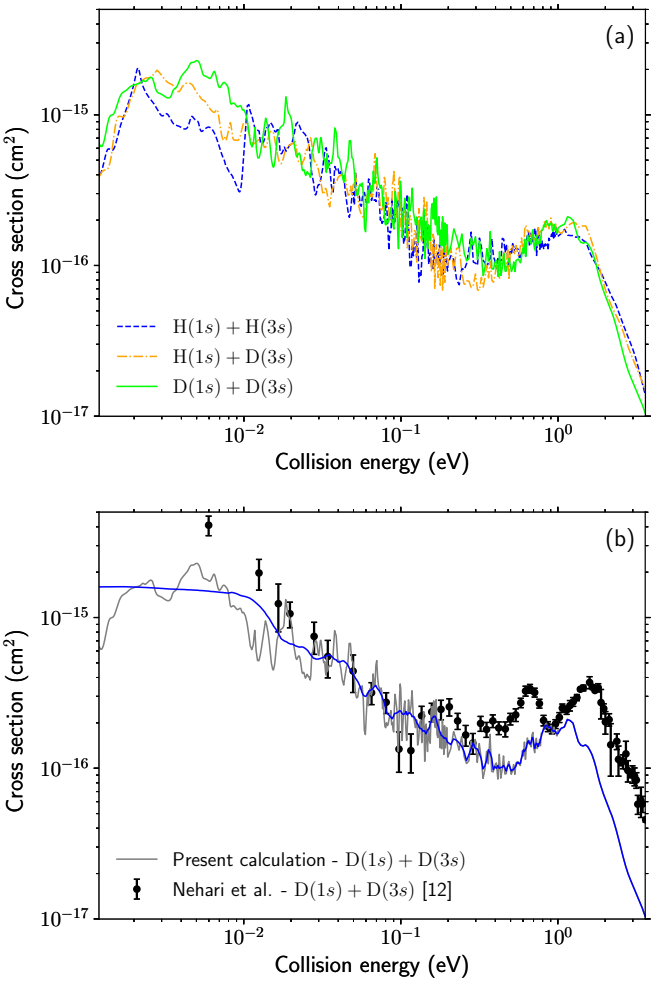

FIG. 9. In (a), the calculated $3s$ AI cross section is compared for different isotopes of atomic hydrogen. In (b), the calculated $D(1s) + D(3s)$ AI cross section (solid gray) is compared with the experimental result of Ref. [12]. The cross section averaged over the experimental energy resolution is shown in solid blue.

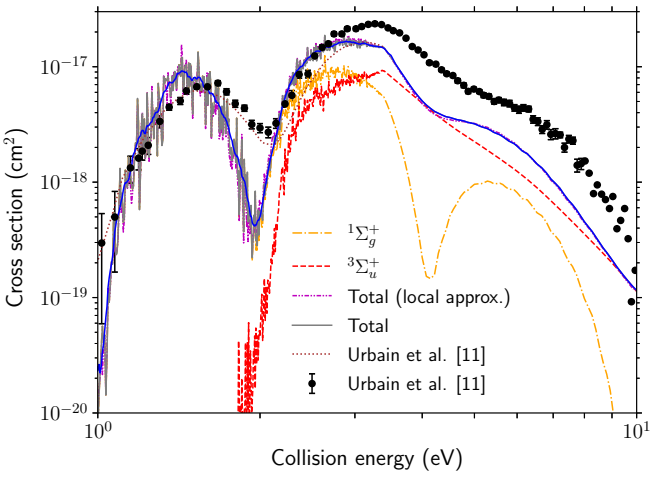

FIG. 10. Calculated $H(1s) + H(2s)$ AI cross section in comparison with the experimental and theoretical results of Ref. [11]. The smoothed (solid blue) curve is the total (nonlocal) cross section averaged over the experimental energy resolution.

interference is also responsible for the third broad peak seen in the $^1\Sigma_g^+$ cross section, which is centered around 5.5 eV. This peak yields a structure in the calculated total cross section which is also seen in the experimental cross section. The second peak of the cross section, centered at about 3.5 eV, is in part due to competition with the collisional ionization process which becomes energetically possible at this energy and in part due to the strong oscillations in the $^1\Sigma_g^+$ cross section.

The present result is in reasonably good agreement with the measurement of Ref. [11], although it underestimates the measured cross section at higher energies. At the 3.5 eV peak, the present result is smaller than the measured cross section by a factor of about 1.4. This could be due to contribution from higher-lying resonant states that were not included in the calculation, or due to the fact that we neglected the contribution from the $^3\Sigma_g^+$ symmetry. The calculated cross section displays sharp resonances, especially at collision energies below 2 eV, which are due to asymptotically closed channels. In Ref. [11], they neglected the $^3\Sigma_u^+$ symmetry due to its relatively high-lying resonant state and its small autoionization width. The present results indicate that this symmetry is important for the $H(1s) + H(2s)$ AI process. Also shown in Fig. 10 is a calculation performed using the local approximation. Although there are only a few vibrational channels open at small collision energies, the difference between the local and nonlocal cross sections is small.

In Fig. 11(a), the calculated $2s$ AI cross section is shown for different isotopes of atomic hydrogen. As the reduced mass of the system is increased, the local minimum which is present at around 2 eV for $H(1s) + H(2s)$ is shifted to lower energies. When one or two hydrogen atoms are replaced with deuterium, one more local minimum appears at around 2.7 eV. This minimum has the same origin as the first local minimum but is less pronounced due to the rapid increase of the $^3\Sigma_u^+$ cross section. This is demonstrated in Fig. 11(b), where we compare the calculated $D(1s) + D(2s)$ cross section to the experimental result of Ref. [3]. The local minimum at 2.7 eV is also present in the experimental cross section. For high collision energies, the present result for the $D(1s) + D(2s)$ cross section is smaller than the experimental cross section (about a factor of 2 at the 3.5 eV peak). Overall, a reasonable agreement is found between the theoretical and experimental cross sections, especially in terms of the structure. The inclusion of higher-lying resonant states in the calculation would likely improve the agreement with the experiment at higher collision energies.

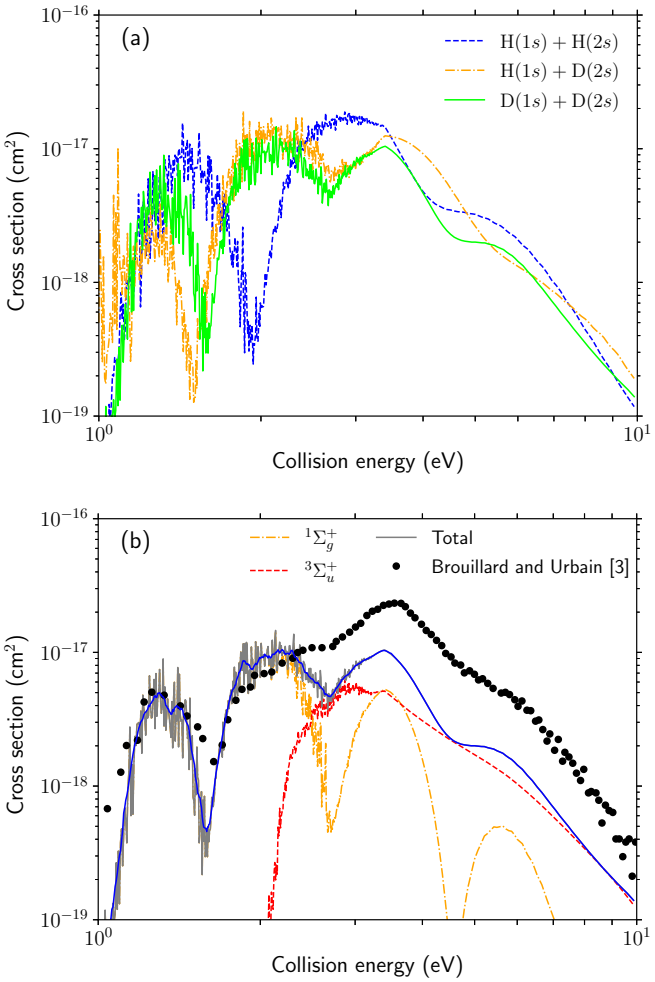

FIG. 11. In (a), the calculated $2s$ AI cross section is compared for different isotopes of atomic hydrogen. In (b), the calculated $D(1s) + D(2s)$ AI cross section (solid gray) is compared with the experimental result of Ref. [3]. The total cross section averaged over the experimental energy resolution is shown in solid blue.

IV. SUMMARY

We have studied associative ionization in collisions of $H^+ + H^-$ and $H(1s) + H(ns)$ with $n = 2, 3, 4$ and we considered contributions from electronic states in the $^1\Sigma_{g/u}^+$ and $^3\Sigma_{g/u}^+$ symmetries. Although $^1\Sigma_g^+$ is the most dominant symmetry at low energies [except in the case of $H(1s) + H(4s)$], the other symmetries contribute significantly at higher energies, and it is therefore crucial that these symmetries are included in the description of these processes. We have investigated the inclusion of covalent states associated with asymptotic limits of $n > 4$. For all the processes considered here, it was found that states up to the $n = 7$ limit needed to be added in order for the cross sections to be converged with respect to the number of states included. Rotational couplings were included in test calculations, but were found to have a negligible influence on the cross sections. Overall, the present results are in good agreement with the experimental data. The exception is process (1) with $n = 4$, likely because we are lacking *ab initio* data of the adiabatic potentials and nonadiabatic couplings for some of the states correlating with the $n = 4$ limit. We have also investigated the importance of a nonlocal description of the AI process. For all processes considered in this paper, it was found that the cross section obtained using the local approximation does not differ significantly from the cross section obtained using a nonlocal complex potential. The isotope effect has been studied by replacing one or two of the hydrogen ions or atoms with deuterium. In general, the cross sections involving the different isotopes have a similar magnitude, but different structures.

The method applied here has previously been applied in the study of mutual neutralization in collisions of H^+ with H^-

[13], but can also be applied to study other processes such as double charge transfer, dissociative recombination, and resonant ion-pair formation, using the same set of potentials and couplings. The model is not limited to the H_2 system, but can also be applied to other diatomic systems for which it is possible to carry out accurate structure calculations of excited states.

ACKNOWLEDGMENTS

The authors would like to thank Xavier Urbain for useful discussions. This work was performed as a part of the project "Probing charge- and mass-transfer reactions on the atomic level," supported by the Knut and Alice Wallenberg Foundation (2018.0028).

[1] M. C. Zammit, M. Charlton, S. Jonsell, J. Colgan, J. S. Savage, D. V. Fursa, A. S. Kadyrov, I. Bray, R. C. Forrey, C. J. Fontes, J. A. Leiding, D. P. Kilcrease, P. Hakel, and E. Timmermans, Phys. Rev. A **100**, 042709 (2019).

[2] E. G. Myers, Phys. Rev. A **98**, 010101(R) (2018).

[3] F. Brouillard and X. Urbain, Phys. Scr. **T96**, 86 (2002).

[4] J. M. Rawlings, J. E. Drew, and M. J. Barlow, Mon. Not. R. Astron. Soc. **265**, 968 (1993).

[5] S. Miller, J. Tennyson, S. Lepp, and A. Dalgarno, Nature (London) **355**, 420 (1992).

[6] A. A. Mihajlov, D. Jevremovic, P. Hauschildt, M. S. Dimitrijevic, L. M. Ignjatovi, and F. Alard, Astron. Astrophys. **403**, 787 (2007).

[7] A. A. Mihajlov, D. Jevremovic, P. Hauschildt, M. S. Dimitrijevic, L. M. Ignjatovic, and F. Alard, Astron. Astrophys. **471**, 671 (2007).

[8] A. A. Mihajlov, L. M. Ignjatovi, V. A. Sre, and S. Dimitrijevi, Astrophys. J. Suppl. Series **193**, 2 (2011).

[9] G. Poulaert, F. Brouillard, W. Claeys, J. W. McGowan, and G. V. Wassenhove, J. Phys. B: At. Mol. Phys. **11**, L671 (1978).

[10] X. Urbain, A. Giusti-Suzor, D. Fussen, and C. Kubach, J. Phys. B: At. Mol. Phys. **19**, L273 (1986).

[11] X. Urbain, A. Cornet, F. Brouillard, and A. Giusti-Suzor, Phys. Rev. Lett. **66**, 1685 (1991).

[12] D. Nehari, F. Brouillard, J. Jureta, and X. Urbain, J. Phys. B: At. Mol. Opt. Phys. **35**, 4733 (2002).

[13] J. Hörnquist, P. Hedvall, Å. Larson, and A. E. Orel, Phys. Rev. A **106**, 062821 (2022).

[14] T. N. Rescigno, C. W. McCurdy, A. E. Orel, and B. H. Lengsfield, III, *The Complex Kohn Variational Method in Computational Methods for Electron-Molecule Scattering*, edited by W. H. Huo and F. A. Gianturco (Plenum, New York, 1995).

[15] Y. I. Kurokawa, H. Nakashima, and H. Nakatsuji, Phys. Chem. Chem. Phys. **21**, 6327 (2019).

[16] J. Weiner, F. Masnou-Seeuws, and A. Giusti-Suzor, Adv. Atom. Mol. Opt. Phys. **26**, 209 (1990).

[17] C. A. Mead and D. G. Truhlar, J. Chem. Phys. **77**, 6090 (1982).

[18] J. Grosser, T. Menzel, and A. K. Belyaev, Phys. Rev. A **59**, 1309 (1999).

[19] A. K. Belyaev, D. Egorova, J. Grosser, and T. Menzel, Phys. Rev. A **64**, 052701 (2001).

[20] A. K. Belyaev, Phys. Scr. **80**, 048113 (2009).

[21] A. K. Belyaev, Phys. Rev. A **82**, 060701(R) (2010).

[22] H. Feshbach, Ann. Phys. **5**, 357 (1958).

[23] H. Feshbach, Ann. Phys. **19**, 287 (1962).

[24] R. J. Bieniek, Phys. Rev. A **18**, 392 (1978).

[25] R. J. Bieniek, J. Phys. B: At. Mol. Phys. **13**, 4405 (1980).

[26] A. Herzenberg, J. Phys. B **1**, 548 (1968).

[27] D. T. Birtwistle and A. Herzenberg, J. Phys. B **4**, 53 (1971).

[28] L. Dube and A. Herzenberg, Phys. Rev. A **11**, 1314 (1975).

[29] L. Dube and A. Herzenberg, Phys. Rev. A **20**, 194 (1979).

[30] B. R. Johnson, J. Chem. Phys. **67**, 4086 (1977).

[31] M. L. Du, Comput. Phys. Commun. **77**, 229 (1993).

[32] A. K. Belyaev, Phys. Rev. A **91**, 062709 (2015).

[33] E. P. Wigner, Phys. Rev. **73**, 1002 (1948).

[34] X. Urbain (private communication).